Synthesis, Structure, and Magnetic Properties of a New Lamellar Iron Phosphonate, $Fe^{II}(C_2H_5PO_3)\cdot H_2O$

Bruno Bujoli,*,† Octavio Pena,§ Pierre Palvadeau,‡ Jean Le Bideau,‡ Christophe Payen,‡ and Jean Rouxel‡

Laboratorie de Synthèse organique, URA CNRS 475, 2 rue de la Houssinière, 44072 Nantes Cedex 03, France; Institut des Matériaux, Laboratoire de Chimie des Solides, UM CNRS 110, 44072 Nantes Cedex 03, France; and Chimie du Solide et Inorganique Moléculaire, URA 254 Avenue du Général Leclerc, 35042 Rennes Cedex, France

Received November 4, 1992. Revised Manuscript Received February 1, 1993

A prolonged reaction between the lamellar iron oxychloride FeOCl and ethylphosphonic acid in acetone leads to a new lamellar iron phosphonate, $Fe^{II}(C_2H_5PO_3)\cdot H_2O$. It crystallizes in space group $P1n1$ ($Z = 2$) with parameters $a = 4.856(8)$ Å, $b = 10.33(1)$ Å, $c = 5.744(3)$ Å, $\beta = 91.0(1)°$. The lamellar structure consists of roughly coplanar layers of iron atoms coordinated octahedrally by five phosphonate oxygen atoms and one water molecule. Mossbauer parameters agree with values given for Fe^{2+} in a high-spin state (isomer shift IS = 1.23 mm s^{-1}). Magnetic susceptibility measurements on a powdered sample shows the compound to be a nearly two-dimensional antiferromagnet with field-induced weak ferromagnetism below $T_c = 24.5$ K, which is probably due to spin canting.

Introduction

Layered transition-metal phosphates and phosphonates have been intensively studied because of the richness of their chemistry and their possible applications in various fields.[1-11] A great interest has been focused on tetravalent metal salts such as the well-known layered zirconium phosphate $Zr(PO_3OH)_2\cdot H_2O$ (α-ZrP).[1,2] More recently vanadyl phosphonates[8] and derivatives of divalent metals $M(II)(RPO_3)\cdot H_2O$[9-10,12] have also been prepared.

In previous papers[13-15] we have demonstrated that trivalent elements form layered phosphonates and described the preparation of two types of iron(III) phosphonates, $HFe(RPO_3H)_4$ and $HFe(RPO_3)_2\cdot H_2O$, in which iron atoms were always found to be in a 3+ oxidation state.

When R = C_2H_5, it appears that $HFe(C_2H_5PO_3)_2\cdot H_2O$ leads after prolonged reflux to a new derivative $Fe(C_2H_5PO_3)\cdot H_2O$ whose Mossbauer spectrum shows iron in a 2+ oxidation state. It is however of interest to note that the preparation of this compound has failed when following the procedure described by Cao et al.[9] (respectively Clearfield and co-workers[12]), starting with ferrous sulfate. An iron 3+ compound, $FeO(C_2H_5PO_3)\cdot 2H_2O$ ($HFe(C_2H_5PO_3)_2\cdot H_2O$), described earlier[15,16] was invariably obtained. Moreover Cunningham et al.[17] reported that despite all efforts to exclude oxygen in reactions between ferrous sulfate and phosphonic acids, products contaminated by iron 3+ were always obtained.

In this paper, we report on the synthesis and the X-ray structural determination, along with some magnetic properties of the title compound.

Experimental Section

Preparation. Iron oxychloride was prepared from Fe_2O_3 and $FeCl_3$ by the usual sealed-tube technique.[18] Ethylphosphonic acid was a commercial reagent (Aldrich). The reaction procedure consisted of sealing 107 mg (1 mmol) of FeOCl, 220 mg (2 mmol) of ethylphosphonic acid, and 5 mL of dried acetone in a Pyrex tube and heating the mixture at 80 °C for 1 month. The white crystalline product was filtered off with suction, rinsed with acetone and dried at room temperature under vacuum (yield 50%).

Crystal Structure Determination. The crystal used was a clear colourless needle of dimensions 0.02 × 0.07 × 0.36 mm^3. Crystal parameters and other data are summarized in Table I.

Data were collected on an Enraf-Nonius CAD4 diffractometer using Mo Kα ($\lambda = 0.710\,69$ Å) with a graphite monochromator. Cell constants on an orientation matrix for data collection were obtained from least-squares refinement, with use of the setting angles of 19 reflections in the range 2-25°. To check on crystal and instrument stability, three representative reflections were measured every 60 min and no decay was observed. The

* To whom the correspondence must be addressed.
† Laboratoire de Synthèse organique.
‡ Institut des Matériaux.
§ Chimie du Solide et Inorganique Moléculaire.

(1) Clearfield, A.; Smith, G. D. *Inorg. Chem.* **1969**, *8*, 431.
(2) Alberti, G.; Constantina, U.; Alluli, S.; Tomassini, J. *J. Inorg. Nucle. Chem.* **1978**, *40*, 1173.
(3) Chalandon, A.; Crisinel, P.; Horriere, D.; Beach, B. G. W. *Proc. Br. Crop. Prot. Conf. Pests. Dis.* **1979**, *2*, 347.
(4) Kodama, Y.; Kodama, T.; Nakabayashi, M.; Senoura, M.; Kiba, Y. Japan Patent No. 7703024.
(5) King, D. L.; Cooper, M. D.; Faber, A.; Schramm, C. M. *Catalytica report*; Molecularly Engineered Layered Structures. Novel Materials for catalysis and surface chemistry, 1988.
(6) DiGiacomo, P. M.; Dines, M. B. *Polyhedron* **1982**, *1*, 61.
(7) Tsvetaeva, N. E.; Rudaya, L. Y.; Fedoseev, D. A.; Ivanova, L. A.; Shapiro, K. Y. USSR Patent No. 623392, 1976.
(8) Johnson, J. W.; Brody, J. F.; Alexander, R. M.; Pilarski, B.; Katritsky, A. R. *Chem. Mater.* **1990**, *2*, 198.
(9) Cao, G.; Lee, H.; Lynch, V. M.; Mallouk, T. E. *Inorg. Chem.* **1988**, *28*, 2781.
(10) Ortiz-Avila, Y.; Rudolf, P.; Clearfield, A. *Inorg. Chem.* **1989**, *27*, 2137.
(11) Cao, G.; Rabenberg, L. K.; Numm, C. W.; Mallouk, T. E. *Chem. Mat.* **1991**, *3*, 149.
(12) Martin, K. J.; Squattrito, P. J.; Clearfield, A. *Inorg. Chim. Acta* **1989**, *155*, 7.
(13) Palvadeau, P.; Queignec, M.; Vénien, J. P.; Bujoli, B.; Villieras, J. *J. Mater. Res. Bull.* **1988**, *23*, 1561.
(14) Bujoli, B.; Palvadeau, P.; Rouxel, J. *Chem. Mater.* **1990**, *2*, 582.
(15) Bujoli, B.; Palvadeau, P.; Rouxel, J. *C.R. Acad. Sci. Paris* **1990**, *310*, 1213.
(16) Bujoli, B. Ph.D. Thesis, Nantes University, 1990.
(17) Cunningham, D.; Hennely, P. J. D.; Deeney, T. *Inorg. Chim. Acta* **1979**, *37*, 95.
(18) Schafer, H. *Z. Anorg. Allg. Chem.* **1949**, *260*, 279.

0897-4756/93/2805-0583$04.00/0

Table I. Crystallographic Data for $Fe(C_2H_5PO_3)\cdot H_2O$

$C_2H_7O_4FeP$	T = 23 °C
a = 4.856(8) Å	λ = 0.710 69 Å
b = 10.33(1) Å	μ = 28.2 cm^{-1}
c = 5.744(3) Å	scan type $\omega/2$
β = 91.0(1)°	scan width 1.50 + 0.25 tan θ
V = 288.0(9) Å^3	data coll range (θ) 1.5–27.5
Z = 2	R = 0.08
space group $P1n1$	R_w = 0.099

Table II. Positional Parameters and B_{eq} Values for the Non-Hydrogen Atoms of $Fe(C_2H_5PO_3)\cdot H_2O$

atom	X	Y	Z	B (Å^2)
Fe	0.0	0.0213(3)	0.0	1.13(4)
P	0.436(1)	0.8362(6)	−0.001(1)	0.93(9)
O(1)	0.749(3)	0.852(2)	−0.002(3)	1.5(3)
O(2)	0.300(3)	0.896(2)	−0.225(3)	1.2(3)
O(3)	0.306(3)	0.901(2)	0.208(3)	1.4(3)
O(4)	0.309(3)	0.183(2)	−0.005(3)	1.5(3)[a]
C(1)	0.347(5)	0.664(3)	0.026(5)	2.4(5)[a]
C(2)	0.459(7)	0.585(4)	−0.195(6)	3.3(6)[a]

[a] Atoms refined isotropically. Anisotropically refined atoms are given in the form of the isotropic equivalent displacement parameters defined as $^4/_3[a^2\beta_{11} + b^2\beta_{22} + c^2\beta_{33} + ab(\cos\gamma)\beta_{12} + ac(\cos\beta)\beta_{13} + bc(\cos\alpha)\beta_{23}]$.

calculated linear absorption coefficient was μ = 28.2 cm^{-1}, and since the crystal was very small no absorption correction was applied. A secondary extinction correction was applied.[19] A total of 708 reflections with $I > 3\ \sigma(I)$ were used for the structure refinement. Iron and phosphorus positions were determined from a Patterson map, and the remaining atoms were located in successive difference Fourier maps. The structure was refined by full-matrix least-squares procedures with anisotropic thermal parameters for P, Fe, and O atoms. All calculations were done using the SDP-PLUS program written by Frenz.[20] The high values of the R factors are likely a consequence of the ethyl groups that probably present static disorder rather than the averaged dynamic disorder given by our refinement. The number of reflections was too low to consider a refinement in a larger unit cell.

Refined positional parameters for non-hydrogen atoms and main bond distances and angles are given in Tables II and III, respectively. A list of structure factors and additional data are available from the authors.

Magnetic and Mossbauer Measurements. Magnetic measurements were performed on a powdered sample. The purity of the sample was carefully checked to avoid the possible presence of a ferromagnetic impurity. To date, we have not succeeded in growing large enough single crystals for anisotropic magnetic experiments. Since an accurate understanding of the magnetism in the orbitally unquenched title compound required single crystal measurements, the conclusions drawn from our results were somewhat quantitatively limited. Static magnetic data were recorded using a commercial SQUID magnetometer. An ac susceptibility experiment was also carried out using a LakeShore ac susceptometer working at H_{ac} = 5 Oe. All measured susceptibilities and magnetizations were corrected for diamagnetism (χ_{dia} was taken equal to -80×10^{-6} emu mol^{-1} using the Pascal's constants) as well as for sample holder contribution.

Mossbauer spectra were obtained on a conventional time-mode spectrometer with constant acceleration drive and a triangular reference signal. Spectra were run until an off-resonance count of 10^6 was reached. The temperature of the absorber was varied by mounting it in an Oxford variable temperature cryostat. The spectra were analyzed by least-squares fitting of Lorentzian lines to the data. Feα was used as reference.

Results and Discussion

Description of the Structure. One surprising feature is that $Fe(C_2H_5PO_3)\cdot H_2O$ crystallizes in a monoclinic space group rather in the orthorhombic one that the zinc and manganese phenylphosphonates adopt. But it is worth noting that Clearfield reported that, although the structures of the zinc and manganese phenylphosphonates were refined in the orthorhombic system, space group $Pmn2_1$, superlattice spots along both a and c axes were found, suggesting that the true unit cell may be a monoclinic lattice, owing to a disorder of the phenyl rings.[21] Moreover this lower symmetry is probably a consequence of a more important disorder in the orientation of the ethyl group, compared with the more symmetric phenyl substituent. In addition this feature is also found for two isostructural copper(II) phosphonates $Cu(RPO_3)\cdot H_2O$ with a monoclinic symmetry for the methyl group while an orthorhombic one is described for the phenyl group.[21]

Table III. Selected Bond Lengths (Å) and Bond Angles (deg) for $Fe(C_2H_5PO_3)\cdot H_2O$[a]

1	2	3	1–2	1–2–3
O(1)a	Fe	O(2)b	2.14(1)	84.5(6)
O(1)a	Fe	O(2)c		97.8(6)
O(1)a	Fe	O(3)b		85.5(6)
O(1)a	Fe	O(3)d		93.5(6)
O(1)a	Fe	O(4)		172.8(7)
O(2)b	Fe	O(2)c	2.35(1)	163.2(7)
O(2)b	Fe	O(3)b		65.2(6)
O(2)b	Fe	O(3)d		92.5(6)
O(2)b	Fe	O(4)		88.9(6)
O(2)c	Fe	O(3)b	2.05(1)	97.9(6)
O(2)c	Fe	O(3)d		104.4(6)
O(2)c	Fe	O(4)		91.6(6)
O(3)b	Fe	O(3)d	2.26(1)	157.7(7)
O(4)	Fe	O(3)b	2.24(1)	89.0(6)
O(3)d	Fe	O(4)	2.07(1)	89.8(6)
O(1)	P	O(2)	1.53(1)	111.3(8)
O(1)	P	O(3)		112.6(8)
O(1)	P	C(1)		109.7(8)
O(2)	P	O(3)	1.57(1)	107.2(8)
C(1)	P	O(2)	1.84(2)	110.9(8)
O(3)	P	C(1)	1.52(1)	104.9(8)
C(2)	C(1)	P	1.61(3)	110(2)

[a] Symmetry operators: (a) $x-1, y-1, z$; (b) $x, y-1, z$; (c) $x-{}^1/_2, 1-y, z+{}^1/_2$; (d) $x-{}^1/_2, 1-y, z-{}^1/_2$.

Figure 1 shows the structure of $Fe(C_2H_5PO_3)\cdot H_2O$ viewed down the stacking axis c (a) and down the b axis (b), respectively. The layered arrangement appears clearly to be the same as in the structures of $Mn(C_6H_5PO_3)\cdot H_2O$ and $Zn(C_6H_5PO_3)\cdot H_2O$.[9,12] Polar groups (phosphonate, oxygen, and lattice water) form a two-dimensional network in which the metal atoms are nearly coplanar. The P–C bonds are approximately perpendicular to these metal planes, and the ethyl groups make van der Waals contacts between layers. The coordination around the metal atom is a distorted octahedron of oxygen atoms. Five coordinated sites are occupied by phosphonate oxygens, and the sixth one is occupied by the water oxygen. One of the phosphonate oxygen bonds to only one Fe atom, and the two others bond to two Fe atoms. One of the cis O–Fe–O angles in the Fe–O6 octahedron is small (65.2°; 63.6° for $Mn(C_6H_5PO_3)\cdot H_2O$, and 64.5° for $Zn(C_6H_5PO_3)\cdot H_2O$) because the two oxygen atoms are bonded to the same phosphorus. Curiously this structural type is very close to the FeOCl one with similar corrugated Fe–O–Fe arrangements. But in this iron ethylphosphonate there is only one Fe–O sheet separated by the phosphonate moieties.

(19) Zachariasen, W. H. *Acta Crystallogr.* **1963**, *16*, 1139.
(20) Frenz, B. A. *Enraf Nonius Structure Determination Package*; Delft University Press: Delft, Holland, 1985.
(21) Zhang, Y.; Clearfield, A. *Inorg. Chem.* **1992**, *31*, 2821.

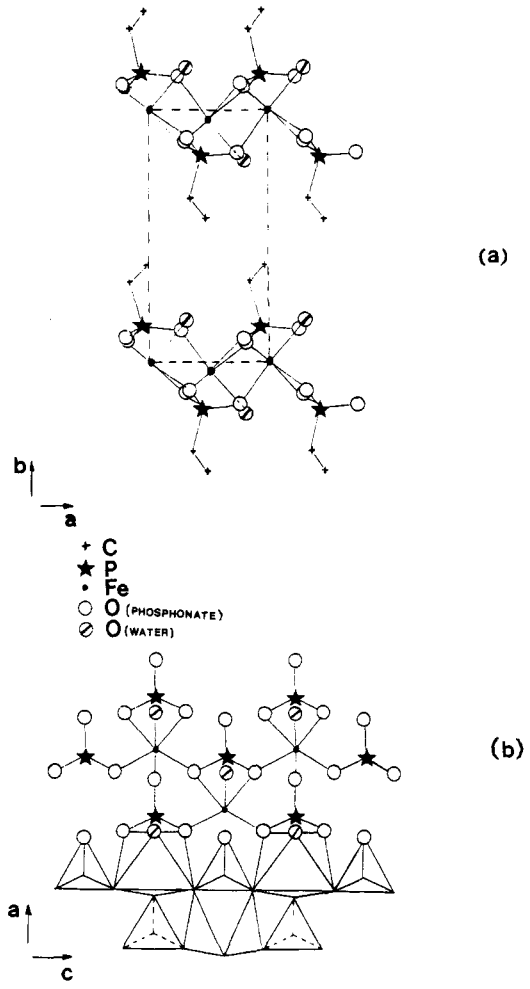

Figure 1. Structure of $Fe(C_2H_5PO_3)\cdot H_2O$ viewed down the stacking axis c (a) and the b axis (b). In (b) carbon atoms have been omitted for clarity.

Unlike most of the compounds of the $M^{II}(RPO_3)\cdot H_2O$ series (M = Co, Zn, Ni, Mg)[22,23] for which the first weight loss on TGA data exactly corresponds to the loss of coordinated water, in the case of $Fe^{II}(C_2H_5PO_3)\cdot H_2O$, this removal of water (T = 140 °C) is concomitant to the oxidation of the iron. The Mossbauer spectrum of the resulting compound indicates the presence of iron 3+ only (isomer shift = 0.38 mm s^{-1}). Moreover infrared spectroscopy and X-ray energy dispersive spectroscopy show that the ethyl group is still present and that the Fe:P ratio remains unchanged.

Magnetic Study

Results. The temperature dependence of the magnetic susceptibility χ is shown in Figure 2. The powdered sample was zero-field cooled to 2 K and then heated to 300 K in a static applied field of 5 kOe. The $1/\chi$ plot of Figure 3 shows that a Curie–Weiss law is obtained in the high-temperature range 180–300 K. The Curie constant and effective moment are C = 3.9 emu K^{-1} mol^{-1} and μ_{eff} = 5.5 μ_B. These values are consistent with high-spin Fe^{2+}. This result is supported by the Mossbauer parameters. At 300 and 77 K the experimental values are respectively isomer shift (IS) = 1.23 and 1.30 mm s^{-1} and quadrupole splitting ΔE = 1.52 and 2.92 mm s^{-1} (Figure 4). The Weiss constant

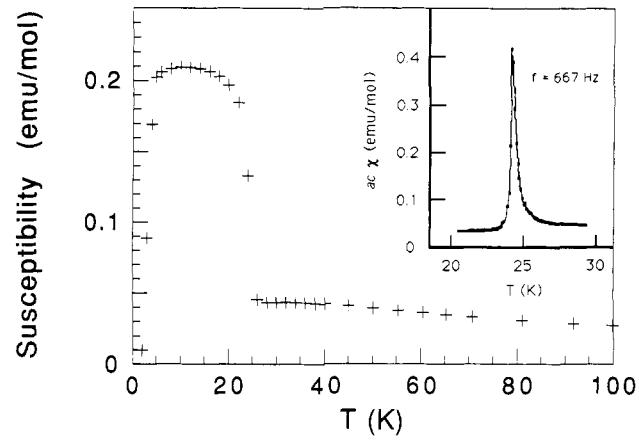

Figure 2. Temperature dependence of magnetic susceptibility of powdered $Fe(C_2H_5PO_3)\cdot H_2O$ at H = 5 kOe. The insert shows the in-phase ac susceptibility obtained at H_{ac} = 5 Oe and f = 667 Hz.

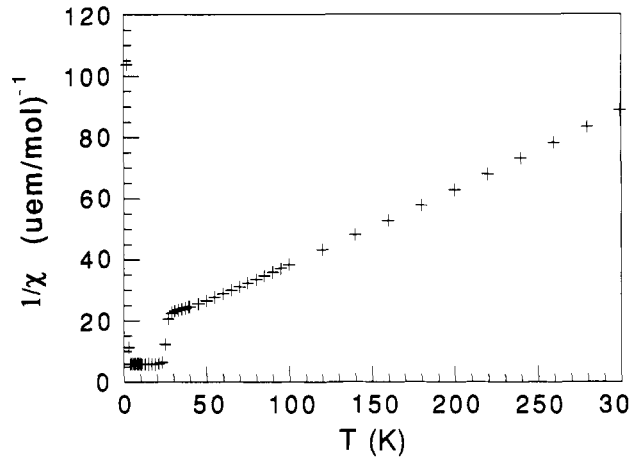

Figure 3. Temperature dependence of the reciprocal susceptibility $1/\chi$ of powdered $Fe(C_2H_5PO_3)\cdot H_2O$ in the range 2–280 K.

value θ_p = −43 K indicates that the predominant interactions between neighbouring iron are of the antiferromagnetic type. Deviation from the Curie–Weiss law occurs below 180 K (lower χ (Figure 3)) and a broad maximum characteristic of low-dimensional antiferromagnets is observed near 35 K with $\chi_{max} \sim 0.04$ emu mol^{-1} (Figure 2). From about 25 K the susceptibility sharply increases up to $\chi \sim 0.2$ emu mol^{-1} and then remains almost constant down to 5 K. This, along with the sharp peak observed at 24 K in the in-phase ac susceptibility χ' (Figure 2) indicates the onset of a 3D weak ferromagnetic ordering. From the point of maximum slope in the χ' vs T curve the transition temperature is estimated as T_c = 24.5 K. Below 5 K the susceptibility χ drops to zero (Figure 2).

Figure 5 shows the magnetization as a function of the applied field at several temperatures below T_c. Data recorded in the paramagnetic state (T = 30 K) are also reported. After every run at a temperature below T_c the sample was heated up to the paramagnetic region and then zero-field cooled to the next selected temperature. The paramagnetic isothermal (T = 30 K) magnetization exhibits the expected linear variation of the magnetization vs the applied field. Below T_c the magnetization increases slowly up to a threshold value H_T where it rises to about 0.16 μ_B/Fe atom. This corresponds to the saturation of the weak ferromagnetic moments. From there a linear increase characteristic of the antiferromagnetic regime is obtained, and no field-induced magnetic phase transition

(22) Cao, G.; Mallouk, T. E. *Inorg. Chem.* **1991**, *30*, 1434.
(23) Frink, K. J.; Wang, R. C.; Colon, J. L.; Clearfield, A. *Inorg. Chem.* **1991**, *30*, 1438.

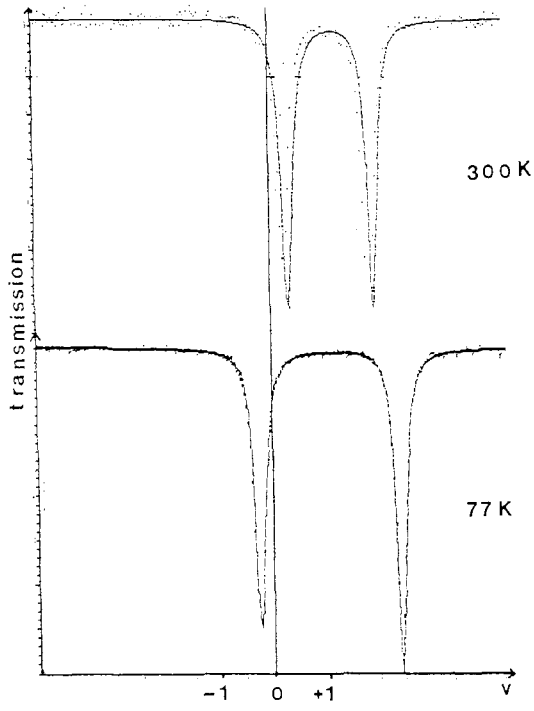

Figure 4. Mossbauer spectra of $Fe(C_2H_5PO_3)\cdot H_2O$, recorded at 300 and 77 K (Feα taken as reference, transmission given in arbitrary units).

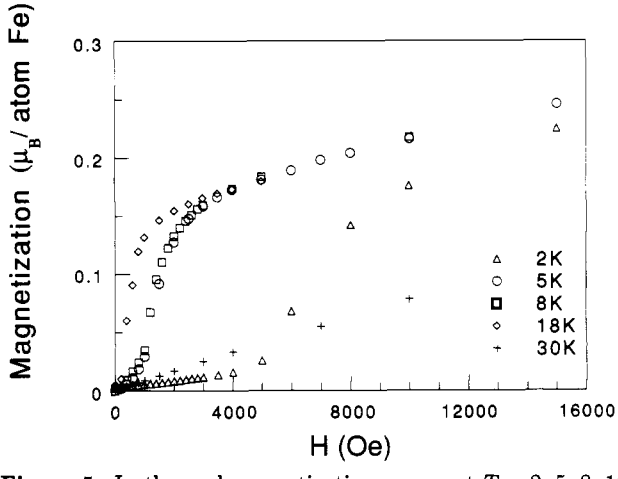

Figure 5. Isothermal magnetization curves at T = 2, 5, 8, 18, and 30 K.

is observed up to the maximum field of 50 kOe available in these experiments. The threshold field decreases with increasing temperatures, being approximately H_T = 6000 Oe, 2000 Oe, 1000 Oe, 500 Oe for T = 2, 5, 8, 18 K respectively. Note that cuts at H = 5 kOe in the isothermal magnetization curves explain the temperature dependence of χ below T_c.

Discussion. We first discuss the origin of the low-dimensional antiferromagnetic properties. From the X-ray diffraction study, it was found that the Fe ions are distributed according to a quasi 2D square lattice in a slab of the structure. Within the layers each Fe(II) has four first neighbors with d_{Fe-Fe} = 3.78 Å. The shortest interplanar Fe–Fe distance is 10.33 Å. From this, along with the large number of nonmagnetic atoms involved in any interslab magnetic path, one expects the interlayers interaction to be much weaker than the intralayer exchange, resulting in the observed 2D properties.

Antiferromagnetism probably arises from magnetic interactions between nearest neighboring iron ions that take place via two different nearly 180° Fe–O–Fe superexchange paths. These two paths correspond to O1a–Fe–O4 = 172.8°, d_{Fe-O} = 2.14 and 2.24 Å and O2b–Fe–O2c = 163.2°, d_{Fe-O} = 2.05 and 2.35 Å (see Table III). Thus each Fe ion is connected a priori nonequivalently to four nearest neighbors within a slab. Hence the calculation of an exchange parameter J using the method of high-temperature series (HTS) expansion (which is usually quite appropriate for 2D systems) is not possible since it can be used only if each magnetic ion is surrounded by first neighbors whose couplings have both the same sign and magnitude. Moreover we did not reach the spin dimensionality of the compound from our powder experiments. However the χ_{max}, $T(\chi_{max})$ HTS predictions do not change drastically from the Ising to Heisenberg limit, while up till now no predictions are available for the $S = 2XY$ case.[24] Assuming that the two different in-plane interactions have both the same sign and magnitude and taking S = 2, g = 2.0, χ_{max} = 0.04 emu mol^{-1}, and $T(\chi_{max})$ = 35 K, the value $J/k_B \sim 5$ K is derived from the HTS results (for a spin Hamiltonian $H = JS_1S_2$). This estimation is also altered by the increase of the susceptibility just above T_c, which is as expected for a weak ferromagnet[25] and which causes the broad 2D maximum to be non-well-defined.

Next we turn to the behavior observed below T_c. This behavior can be explained by the presence of weak ferromagnetic moments due to spin canting. Since both the magnetization and ac susceptibility measurements reveal that there are no saturation effects in low fields ($H < H_T$), we could deal with hidden canting of several (more than two) antiferromagnetic sublattices, and jumps in the isothermal magnetization curves could be explained by a reversal of the directions of part of the spins, the canted moments being now arranged in a fashion such that there is a net moment (overt canting). Alternately, this low-field behavior below T_c could be due to domain formation. Anyhow, the canting angle γ can be calculated from the jump ΔM in the magnetization curves by means of the simple relation $tg\gamma = \Delta M/g\mu_B S$. With $\Delta M = 0.15\,\mu_B$, taking g = 2.0 and S = 2, we get $\gamma \approx 2°$. The presence of spin canting is probably related to the tilted $Fe-O_6$ octahedra in the crystal structure. Actually the adjacent octahedra along the [101] and [10$\bar{1}$] directions are successively tilted with respect to each other. There are symmetry restrictions that apply to canting mechanisms.[24] In particular, ions with magnetic moments in a unit cell cannot be related by a center of symmetry if canting is to occur. On the basis of our X-ray diffraction study, canting is indeed symmetry-allowed in the title compound.

Conclusion

This compound represents a new and interesting situation in the field of iron phosphonates with differences concerning the oxidation state of iron (2^+ instead of 3^+) and the nature of the skeleton of the slabs. The slabs are similar to those of FeOCl with corrugated Fe–O–Fe layers and not a succession of M–O–P–O–M as in α-ZrP.

(24) Navarro R. In *Magnetic properties of layered transition metal compounds*; Physics and Chemistry of Materials with Low-Dimensional structures, Vol. 9; de Jongh, L. J., Ed.; Kluwer Academic Publishers: Dordrecht, Holland, 1990.

(25) Moriya T. In *Magnetism*; vol. I, Rado, G. T., Suhl, J., Eds.; Academic Press: New York.

$Fe^{II}(C_2H_5PO_3)\cdot H_2O$ is closer to the FeOCl–VOCl framework than the other iron(III) phosphonates previously described.[13-15]

The paramagnetic properties of $Fe(C_2H_5PO_3)\cdot H_2O$ are those of a nearly two-dimensional antiferromagnet with unknown spin dimensionality. The weak ferromagnetism observed below T_c is probably due to spin canting. Anisotropic magnetic measurements and determination of the average magnetic structure from neutron scattering will help to get a deeper insight into the origin of the magnetic behavior.

Acknowledgment. We thank Dr. Peter Day for fruitful discussions. This work has been supported by the Commission of European Communities under Contract MA1E-0030-C.